Composites Part B 158 (2019) 218–229

Contents lists available at ScienceDirect

Composites Part B

journal homepage: www.elsevier.com/locate/compositesb

Investigation of the interphase between recycled aggregates and cementitious binding materials using integrated microstructural-nanomechanical-chemical characterization

Mahdieh Khedmati[a], Yong-Rak Kim[b,*], Joseph A. Turner[c]

[a] Department of Civil Engineering, 362 Whittier Research Center, University of Nebraska-Lincoln, Lincoln, NE, 68583-0856, USA
[b] Department of Civil Engineering, 362N Whittier Research Center, University of Nebraska-Lincoln, Lincoln, NE, 68583-0856, USA
[c] Department of Mechanical and Materials Engineering, W342 Nebraska Hall, University of Nebraska-Lincoln, Lincoln, NE, 68583-0856, USA

ARTICLE INFO

Keywords:
Cementitious composites
Recycled aggregate
Geopolymer
Interphase/interface

ABSTRACT

The mixtures including crushed recycled aggregates have multiple complex aggregate/paste interphase regions compared to conventional concrete mixtures, which brings significant technical challenges in understanding and characterization of their properties. To gain a better understanding of such complex material organization, this study adopted multiscale experimental methods by using nanoindentation test-analysis, laser scanning microscopy, and energy dispersive spectroscopy. The multiscale methods were applied to two different composites in which the same recycled aggregates were mixed with two different cementitious binders: a fly ash-based geopolymer and conventional Portland cement. The test-analysis results demonstrate that, in cement concrete mixtures with recycled aggregates (CCRA), the pre-existing incomplete interphase within the recycled aggregares was observed, although new paste was relatively well-bonded to the old recycled aggregate paste by having an approximately 20-μm thick interfacial transition zone. In geopolymer concrete mixtures with recycled aggregates (GCRA), both the old and new interphase appeared dense. More interestingly, the pre-existing incomplete interphase within the recycled aggregates was filled in the GCRA, which was not the case observed from the CCRA. Further analysis using energy dispersive spectroscopy suggests that geopolymeric materials can reach the pre-existing incomplete interphase and create hydration-geopolymerization products that combine calcium-silicate-hydrate (C-S-H) and sodium aluminosilicate hydrate (N-A-S-H) gel. The resulting cementitious composite is expected to show enhanced mechanical properties owing to a better interphase region.

1. Introduction

Construction and demolition wastes (C&DW) are the excess or waste materials produced during the construction, renovation, and demolition of structures and buildings. The disposal of concrete structures and pavements contributes a considerable fraction of C&DW in many countries and induces environmental burdens [1]. Owing to the high cost of raw materials and natural resources, several studies are being conducted globally to search for new low-cost materials that exhibit durability and good performance. Recycled aggregate is a reusable mixture of aggregate and old cement paste that is generated by removing, crushing, and processing old concrete structures that are considered to be beyond their useful life. Recently, the use of recycled aggregate to manufacture new concrete has gained considerable attention in an attempt to reduce the use of virgin materials, to increase economic benefits, and to promote environmental friendliness. Many studies have investigated the engineering properties of recycled aggregate and the effect of using recycled aggregate on the properties of fresh and hardened concrete [2–7]. It is reported that at a high water-to-cement (w/c) ratio of 0.55–0.75, the strength of concrete with recycled aggregates is comparable to that of conventional concrete even at 75%–100% replacement. However, by reducing the w/c ratio to about 0.4, only 25% reduction in the strength compared to the reference mix was observed [8,9]. The properties of recycled aggregates acquired from crushed concrete have a significant effect on the mechanical properties of high-strength concrete [10].

The production of Portland cement, which is the primary component of concrete, is responsible for high levels of CO_2 emissions, and the cement industry alone contributes to about 7% of the entire global CO_2 emissions [11]. One of the efforts to reduce greenhouse gas emissions and to produce more eco-friendly concrete is the use and/or development of inorganic alumina-silicate materials (e.g., geopolymer),

* Corresponding author.
E-mail addresses: mahdieh.khedmati@huskers.unl.edu (M. Khedmati), yong-rak.kim@unl.edu (Y.-R. Kim), jaturner@unl.edu (J.A. Turner).

https://doi.org/10.1016/j.compositesb.2018.09.041
Received 13 July 2018; Received in revised form 17 September 2018; Accepted 19 September 2018
Available online 20 September 2018
1359-8368/

synthesized from industrial by-products such as fly ash that is rich in silicon and aluminum [12]. In geopolymerization, the raw material is transformed into a paste by using a high alkaline solution which is usually a combination of sodium or potassium silicate and sodium or potassium hydroxide [13]. Geopolymer binders can deliver approximately 80% less CO_2 emissions compared to ordinary Portland cement (OPC) [14,15]. Fly ash-based geopolymer paste can be used as an alternative to cement paste for producing concrete, since it can significantly decrease the greenhouse gas emissions and consume a large amount of industrial wastes.

Many studies have investigated the properties of fly ash-based geopolymer and shown that geopolymer has advantages of low creep, high compressive strength, strong bonding to the aggregate, low shrinkage, excellent resistance to sulfate attack, high acid resistance, and great fire resistance [16–20]. Nanomechanical and microstructural characterization of the aggregate-paste interphase in geopolymer concrete mixtures made with natural aggregates have shown that the aggregate surface and paste are usually bonded together tightly due to the formation of sodium aluminosilicate hydrate (N-A-S-H) gel, which is the main reaction product of fly ash-based geopolymer [21,22]. It is reported that, in conventional OPC concrete, there is a weak zone between the aggregate and cement paste which is prone to damage and degradation and is called interfacial transition zone (ITZ) [23–27].

As illustrated in Fig. 1, concrete mixtures including crushed recycled aggregates have multiple complex aggregate-paste interphases compared to conventional concrete mixtures, which leads to significant challenges in understanding and characterization of the concrete properties. There are a number of aggregate-paste interphases within a single recycled aggregate, and the recycled aggregate adheres to a new paste. This organization subsequently leads to different interphases: old interphases between the old aggregates and the adhered old cement paste, and new interphases between the old cement paste and the new cement paste [28,29]. The failure behavior of the concrete mixtures with crushed recycled aggregates depends on the relative quality of the old and new interphases [30]. The lower strength is typically owing to the presence of weak ITZs and old adhered paste [29]. Although it is generally reported that the adhered old paste or the old ITZ is the weakest zone [31], other studies have shown that the adhered old paste is not always the main factor controlling the quality of the entire concrete mixtures with recycled aggregates [32], and the relative strength of the old paste and new paste is the main factor that might define the weakest link [33]. Other studies have measured the nanomechanical properties of both old and new ITZs in cement concrete mixtures made with recycled aggregates by conducting nanoindentation and microhardness tests. Based on their results, the old ITZ showed lower indentation modulus than the old paste matrix, and new ITZ also showed lower indentation modulus than the new paste [30,34]. Regarding geopolymer mixtures with recycled aggregates, limited studies have characterized the new and old interphases [36,37]. Liu et al. [35] conducted microstructural characterization of only the new ITZ in geopolymer concrete mixtures with recycled aggregates and found that a weak ITZ does not develop.

2. Research objectives and scope

In this article, the complex interphases between recycled aggregates and cementitious binding materials are investigated in order to improve the understanding of the interaction between two recycled materials, namely fly ash (an industrial by-product) and recycled aggregates. To meet the research objective, recycled aggregates were mixed with two different cementitious materials to produce two concrete mixtures: geopolymer concrete with recycled aggregates (GCRA hereafter) and cement concrete with recycled aggregates (CCRA hereafter). This study used multiscale experiments (spanning the nano-to-micro scales) by integrating microstructure examination using a laser scanning microscope (LSM), nanomechanical characterization using a nanoindentation test-analysis, and spatial mapping of chemical elements using energy dispersive spectroscopy (EDS).

3. Materials and sample preparation

3.1. Materials and mixture ratios

In this study, low-calcium fly ash (Class F) with specific gravity of 2.37 obtained from Boral, Colorado was used as an aluminosilicate source material for synthesizing the geopolymer. The fly ash chemical composition is presented in Table 1. To activate fly ash particles, an alkaline activator solution was prepared by blending sodium hydroxide (NaOH) and sodium silicate (Na_2SiO_3) solutions. Sodium hydroxide pellets with a purity of 98% were dissolved in distilled water to prepare sodium hydroxide solution of 12 molar concentration. The chemical composition of the sodium silicate solution was 9% Na_2O, 28% SiO_2, and 63% water. The activator solution was allowed to equilibrate for a minimum of 24 h at room temperature prior to use. The mass ratio of the NaOH to Na_2SiO_3 solutions was 1.0. As a counterpart of the fly ash-based geopolymer paste, Type I OPC, with chemical compositions as listed in Table 1, was used to produce cement paste. The water absorption capacity and specific gravity of the recycled aggregates were 6% and 2.40, respectively. Recycled aggregates retained on 4.75, 9.5, and 12.5 mm sieves were used in the mixes.

The ratio of alkali solution to fly ash was 0.4 for fabricating GCRA specimens. The fly ash, recycled aggregates, and alkaline solution content were 706 kg/m^3, 1200 kg/m^3, and 282 kg/m^3, respectively. To prepare GCRA, first, the recycled aggregates in saturated surface dry condition and fly ash were blended for 3 min. Afterward, the alkaline solution was added to the blend of recycled aggregates and fly ash. The obtained mixture was mingled for another 5 min and then was cast in cylinder mold. A curing process at 60 °C in an oven was employed for the GCRA specimens for 24 h. Then the demolded specimens kept at a temperature of 23 ± 2 °C for 28 days. The CCRA specimens were

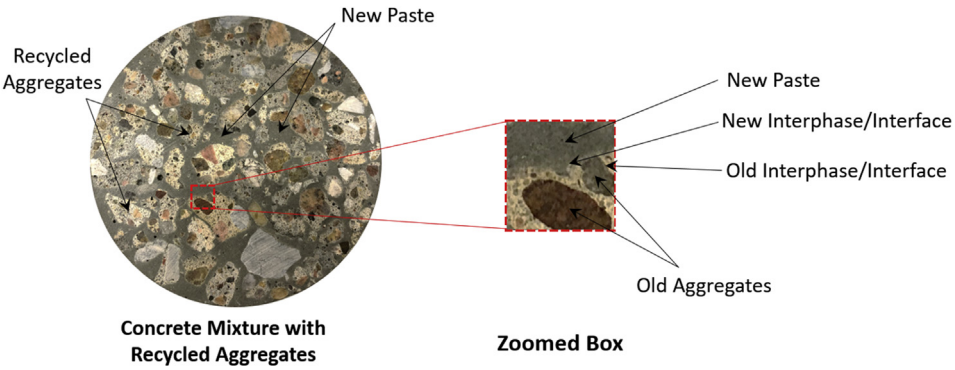

Fig. 1. Schematic illustration of concrete mixture with recycled aggregates.

Table 1
Chemical composition (in % mass) of fly ash (Class F) and Portland cement (Type I).

Component	SiO_2	Al_2O_3	Fe_2O_3	CaO	MgO	K_2O	SO_3	Na_2O	Na_2O_3	LOI
Fly Ash	51.82	23.07	13.02	2.79	0.85	2.52	1.23	2.29	–	2.41
Cement	20.99	6.19	3.86	65.96	0.22	0.6	0.55	–	0.17	1.46

Note: LOI (loss on ignition).

fabricated with water to cement (w/c) ratio of 0.4. The cement, recycled aggregates, and water content for making CCRA were 702 kg/m^3, 1193 kg/m^3, and 281 kg/m^3, respectively. The CCRA specimens had different curing regime, in which after casting, the specimens were sealed by means of lids and plastic bags for 24 h to avoid excessive moisture loss. Then the CCRA specimens were taken out from the mold and kept in water for 28 days. The mixtures were tested for compressive strength, which resulted in the average compressive strength values of three samples for GCRA (34.24 ± 0.85 MPa) and CCRA (33.02 ± 1.29 MPa), respectively. The workability of fresh mixes was also measured via slump flow according to ASTM C143. The results showed that the CCRA mix had slump flow of approximately 55 mm and the GCRA mix had slump flow of approximately 44 mm. The lower workability of GCRA is due to the higher viscosity of alkaline solution compared to water.

3.2. Specimen preparation

In order to obtain accurate results from nanoindentation experiments, it is critical to obtain a flat surface by smoothening and reducing the roughness to an acceptable level [38]. Therefore, 20-mm thick slices from the center part of the cured mixture were extracted. Using a digital low-speed diamond saw, the extracted slice was cut to obtain a small specimen with about 1 cm × 1 cm cross section and 0.4 cm thickness. In order to protect the microstructure of the specimens from the stresses induced by mechanical polishing, which is essential to obtain an extremely flat surface, the specimens were vacuum impregnated using a low viscosity LR White epoxy resin. As the epoxy hardens, the pores and cracks are filled and the microstructure is maintained [39]. After epoxy impregnation, the specimens were ground using silicon-carbide-coated papers (340, 400, 600, 800, and 1200 grit) in an automatic grinder-polisher for 3 min at each step. After the grinding process, the specimens were cleaned in an ultrasonic cleaner. Subsequently, to make sure the uneven surfaces were removed first, 3 μm and 1 μm grade diamond lapping films were used. Furthermore, in order to remove any scratches resulting from previous steps, a series of sequentially finer alumina suspensions (1 μm, 0.3 μm, and 0.05 μm particle diameters) were used to polish the surface. Each step continued about 30 min. Finally, an ultrasonic cleaner was used for 5 min to remove all remaining debris.

4. Testing methods

4.1. Laser scanning microscope (LSM)

To acquire high-resolution images of each specimen microstructure, a laser scanning microscope (LSM) was employed. The LSM is a type of optical microscope that not only collects optical images, but also provides high-resolution surface data by combining a laser light source with white light [40]. In LSM, the specimen is scanned by using a focused laser beam. The intensity that is reflected by the laser beam is produced as a function of position, and as a result, a high-resolution image of the specimen is obtained. The surface topography can be obtained at any area of the sample by analyzing the returned laser light intensity relative to the laser z-position [41,42].

4.2. Energy dispersive spectroscopy (EDS)

A FEI Nova NanoSEM scanning electron microscope (SEM) with energy dispersive X-ray spectroscopy (EDS) was used for qualitative chemical mapping, quantitative line scans, and point analysis of the regions of interest. Before performing the SEM–EDS analysis, the surface of the specimens were sputter coated with a thin carbon layer to dissipate the excessive charge from the sample without interference with elements of interest [39].

4.3. Nanoindentation testing

A Hysitron Triboindentor with a diamond Berkovich tip was employed to obtain the nanomechanical properties of each specimen. The loading profile was trapezoidal using a quasi-static load-control procedure. The profile included a 10-s loading ramp at a rate of 200 μN/s, a maximum load of 2000 μN followed by 5-s holding to eliminate any creep effect [43], following by a 10-s unloading ramp. A schematic of the load vs. contact depth curve is illustrated in Fig. 2.

By analyzing the slope of the unloading curve ($S = dP/dh$) and using the contact area (A_c) determined from calibration and the indentation depth h [44], the indentation modulus or reduced modulus (E_r) of each indent can be obtained. The relationship is given by

$$E_r = \frac{1}{\beta}\cdot\frac{S}{2}\cdot\frac{\sqrt{\pi}}{\sqrt{A_c}}, \tag{1}$$

where β is a dimensionless parameter that considers the shape of the indenter tip [45].

The elastic modulus (E_s) of the indented material can then be calculated from the measured reduced modulus E_r using the Poisson's ratio of the material tested (ν_s), the Poisson's ratio of the diamond indenter (ν_i), and the Young's modulus of the diamond indenter (E_i), as

$$E_s = \frac{1-\nu_s^2}{\frac{1}{E_r} - \frac{1-\nu_i^2}{E_i}} \tag{2}$$

The hardness can also be determined from Equation (3) where P_{max} is the peak load at the load-displacement curve.

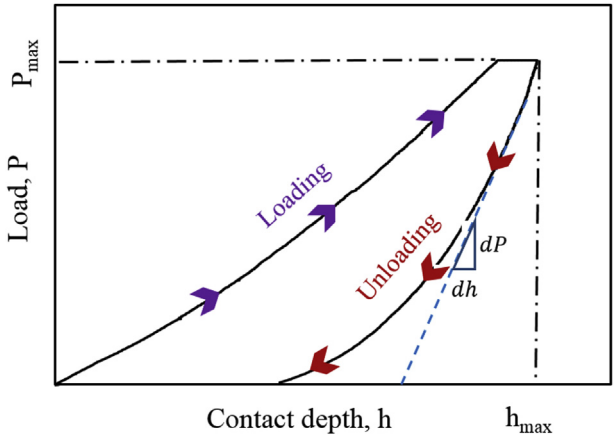

Fig. 2. A Typical nanoindentation load-displacement curve.

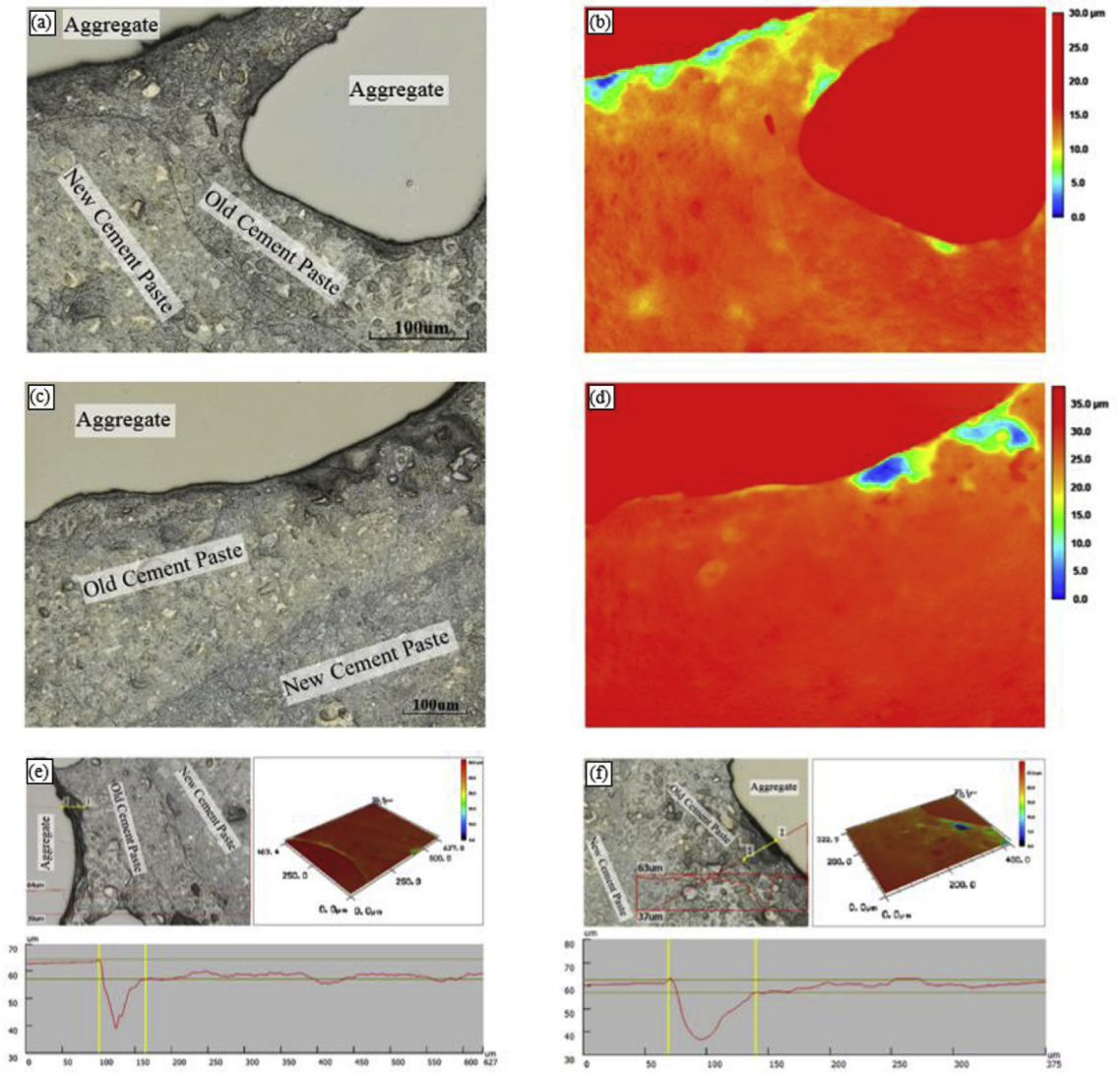

Fig. 3. LSM images of CCRA across old and new interphase: (a) and (c) microstructural images; (b) and (d) topography images; (e) and (f) topographic profiles.

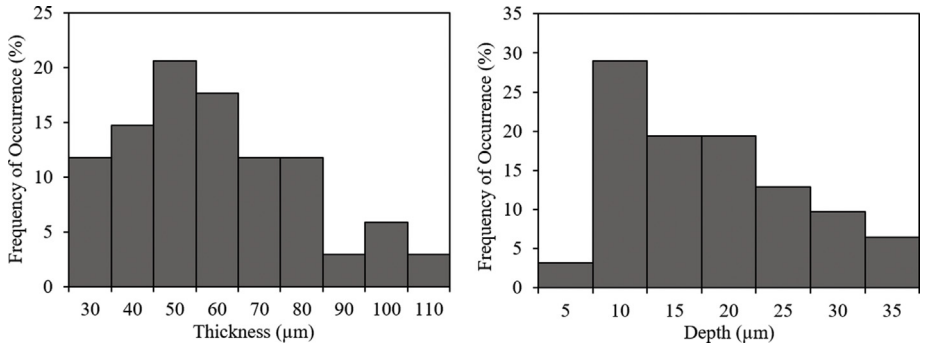

Fig. 4. Frequency of occurrence of thickness and depth of incomplete interfacial zone.

$$H = \frac{P_{max}}{A_c} \tag{3}$$

5. Results and discussion

5.1. Microstructural characterization

Fig. 3 shows the laser scanning microscopy images (3(a) and 3(c)) and topography images (3(b) and 3(d)) taken from regions that include the aggregate, old cement paste, and new cement paste in the CCRA specimen. It can be observed that in some locations, there is a clear interfacial debonding (or separation) with high porosity between the aggregate and old paste. In the topography images, the interfacial debonding (or separation) is clearly seen as the areas around the aggregates that have lower elevation (shown in blue and green) compared to the aggregate phase and paste phase. In contrast, the old paste and new paste appear dense and well-bonded together, and no clear

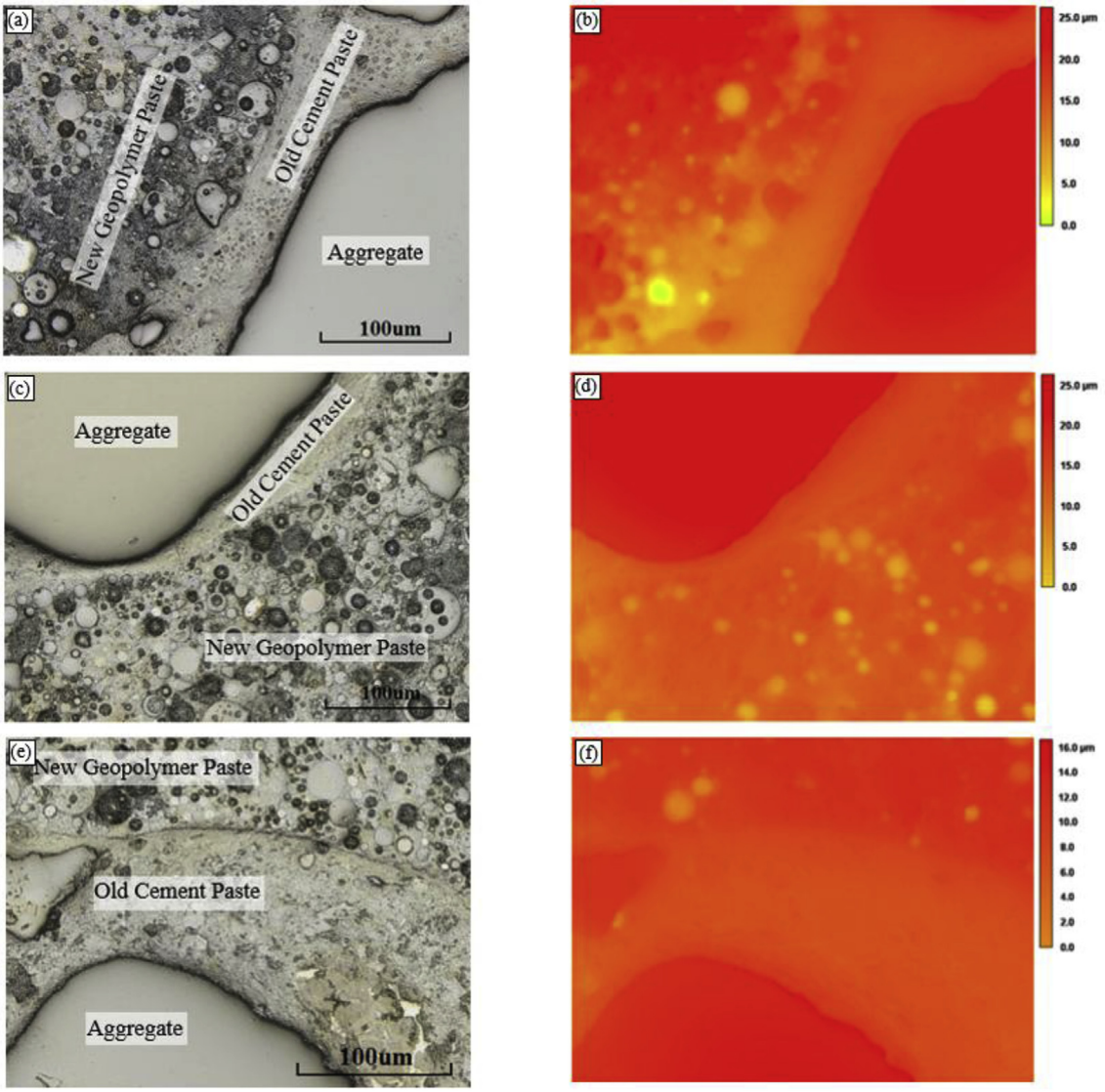

Fig. 5. LSM images of GCRA across old and new interphase: (a), (c), and (e) microstructural images; (b), (d), and (f) topography images.

separation can be observed in the new interphase region. The three-dimensional view and topographic profile of the CCRA specimen across some specific aggregate-old paste-new paste regions are also shown in Fig. 3(e) and (f). The thickness and depth of particular regions where interfacial debonding occurred can be measured from the topographic profiles. The histograms of the thickness and depth of the interfacial debonding, which were captured from 30 different locations on the CCRA specimens, are shown in Fig. 4. As can be inferred, the variation of thickness and depth of the interfacial debonding are in a range of 30–110 μm and 5–35 μm, respectively. The thickness of interfacial debonding observed in CCRA of this study seems larger than that of typical portland cement concrete interphases, which are in the range of 15–50 μm [21].

Fig. 5 shows the LSM and topography images of the GCRA specimen. Similar to CCRA, the old paste and new geopolymer paste appeared well-bonded together. However, the microstructure of the old interphase in GCRA was substantially different from that in CCRA. It was generally viewed that the old paste was very well bonded to the aggregate in most of the old interphase zones. This observation is interesting, because the recycled aggregate particles in both CCRA and GCRA specimens originate from the same source, and thus, a similar microstructural feature from the old interphase region was expected.

In relation to the better interphase zones observed from recycled aggregates in GCRA specimens, it can be noted that some locations around the recycled aggregates in GCRA are in different color contrasts from the adjacent paste (noted as “unknown phase” in Fig. 6), which was detected through optical microscope observations. It can also be implied that, through the contrast image, this region appears relatively denser than the adjacent old paste. To identify the unknown phase, the EDS analysis was conducted to capture elemental (chemical) compositions of the target regions, which are presented later (see sub-section “EDS analysis results” for details).

5.2. Nanomechanical properties

For nanomechanical characterization, areas that contain both old interphase and new interphase were chosen for grid indentation of GCRA and CCRA specimens. The root mean square roughness in multiple areas of both specimens was measured to be 80 nm, which meets the roughness criteria of cementitious materials for nanoindentation test [30]. A total of 609 indents were made, covering 140 μm × 100 μm of the specimen region. The distance between each indent in both the vertical and lateral directions was selected to be 5 μm to avoid any influence between indents. Fig. 7(a) and (b) show the grid indentation patterns and distribution graphs of elastic modulus and hardness captured from the nanoindentation tests on CCRA and GCRA, respectively.

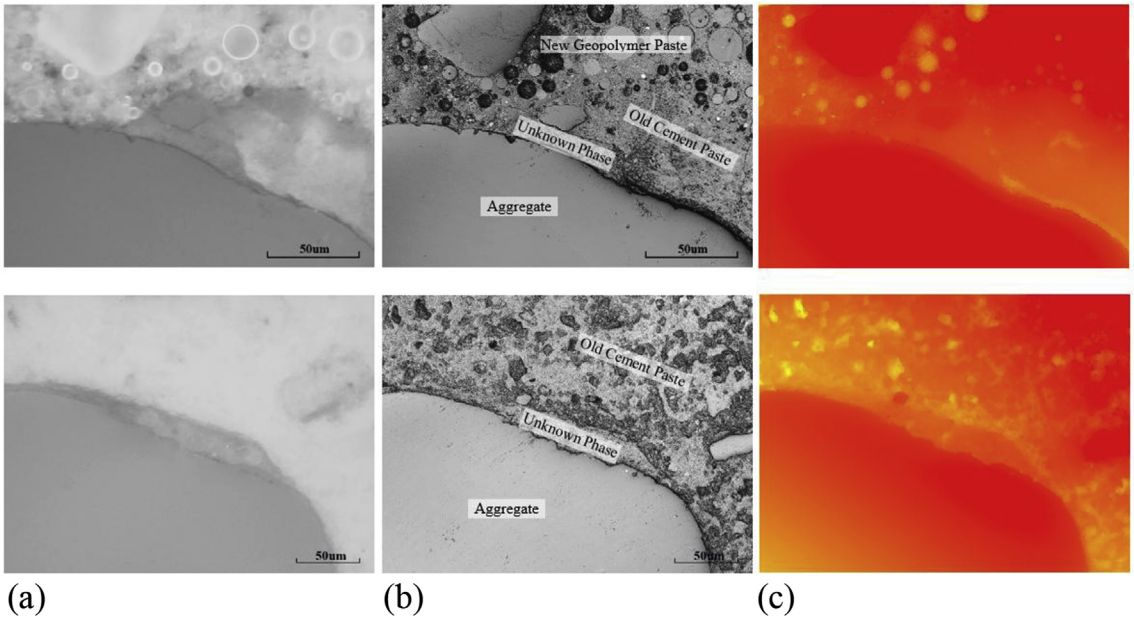

Fig. 6. (a) Optical microscopy images, (b) LSM images, and (c) topography maps of the unknown phase around aggregate in GCRA.

Each bar in the distribution graph shows the average values from 21 indentations with 5 μm spacing in the vertical direction. As mentioned previously, in some areas of the CCRA specimen, the old interphase appeared porous and interfacial debonding/separation was detected between the old aggregate and old paste. Because a smooth surface is required for accurate nanoindentation measurements, the regions with significant interfacial separation in CCRA were intentionally avoided. Fig. 7(a) shows that, when interfacial debonding is not significant between the aggregate and paste, the modulus and hardness of the interphase zone are not very different from the paste region as shown by the modulus bars between 25 and 85 μm. In contrast, the modulus and hardness values of the new cement paste showed an increasing trend between 90 and 110 μm until somewhat consistent values are reached. In order to check if the properties between 90 and 110 μm are statistically different from the properties after 110 μm, the elastic modulus and hardness mean values between the two regions were compared by a *z*-test. The difference in the values of elastic modulus and hardness between the two regions (i.e., region 1: 90 μm–110 μm vs. region 2: 110 μm–140 μm) was significant ($p < 0.01$), as shown in Fig. 8. The average elastic modulus and hardness of region 1 were 22% and 26% lower than that of the region 2, respectively. Region 1 might be related to the formation of a new ITZ within the new cement paste. Regarding the nanomechanical properties of GCRA (Fig. 7(b)), it can be noted that no obvious weak zones are present either in the old interphase or in the new interphase regions. Fig. 7(b) also shows a larger variation of the nanomechanical properties in new geopolymer paste compared to those of the new cement paste which is due to the high heterogeneity of the geopolymer paste.

5.3. EDS analysis results

The chemical elements distribution of CCRA and GCRA was studied by conducting EDS elemental mapping. Fig. 9(a) and (b) show the distribution of each chemical element present on the same regions examined in the previous subsection. The intensity of each color represents the concentration of the related chemical element in the mapped region. Fig. 9(a) shows that the Ca and Si elements are relatively well-distributed in the old cement paste entire region, including the vicinity of the old aggregate. However, in the new cement paste zone, there are regions with a low concentration of Ca and Si and high content of Al. In GCRA (Fig. 9(b)), the distribution map of Na in the new geopolymer paste shows that circular particles appeared dark, which indicates that these particles have low amount of Na. From Table 1, it can be seen that fly ash contains very low amount of Na (2.29%). Thus, it can be inferred that the circular materials are fly ash particles that did not actively react with the alkaline activator. This outcome is because geopolymer paste is likely rich in Na element after active chemical reactions between fly ash particles and an alkaline activator, which is a combination of NaOH and Na_2OSiO_3 solutions. It can also be seen that the large fly ash particles are distributed further away from the surface of the old cement paste, and the three elements (i.e., Na, Al, and Si) are well-distributed in the new geopolymer paste. This result indicates that the main reaction product in geopolymer (i.e., N-A-S-H gel) is well distributed in the new paste, in particular at the region close to the boundary with the old cement paste. The good bonding between the old cement paste and new geopolymer paste observed in the microstructural images (Fig. 5) is supported by the EDS chemical results.

More information about the variation of each chemical element across old aggregate-old paste-new paste can be acquired from the EDS line scanning by focusing on the four elements distribution: Na, Al, Si, and Ca. Analysis results of CCRA and GCRA are shown in Fig. 10(a) and Fig. 10(b), respectively. Fig. 10(a) shows that Ca and Si are well-concentrated close to the boundary of the old aggregate, which suggests the existence of C-S-H within the old interphase. However, in a region approximately 20-μm-wide (from 95 to 115 μm) next to the boundary of the old cement paste, a high concentration of Ca and very low concentration of Si were detected, which might be due to the somewhat large amount of calcium hydroxide (CH) crystals created. This observation agrees well with the general belief of ITZ formation in conventional portland cement concrete, in which the ITZ contains less C-S-H but with a higher amount of CH [24]. It can also be noted that a higher concentration of Al was observed in the new interphase (95–115 μm) compared to the outer paste (115–140 μm), which might be related to the presence of ettringite in the new interphase zone. Several studies have reported an increased amount of ettringite in the ITZ. Monteiro and Mehta [46] claimed the “through-solution” mechanism, which states that aluminate, calcium, and sulfate ions quickly migrate to the surface of the aggregate due to the presence of water film around the aggregate [46].

The EDS test results are compatible with nanoindentation test results shown in Fig. 7(a). Owing to the rich formation of C-S-H, the

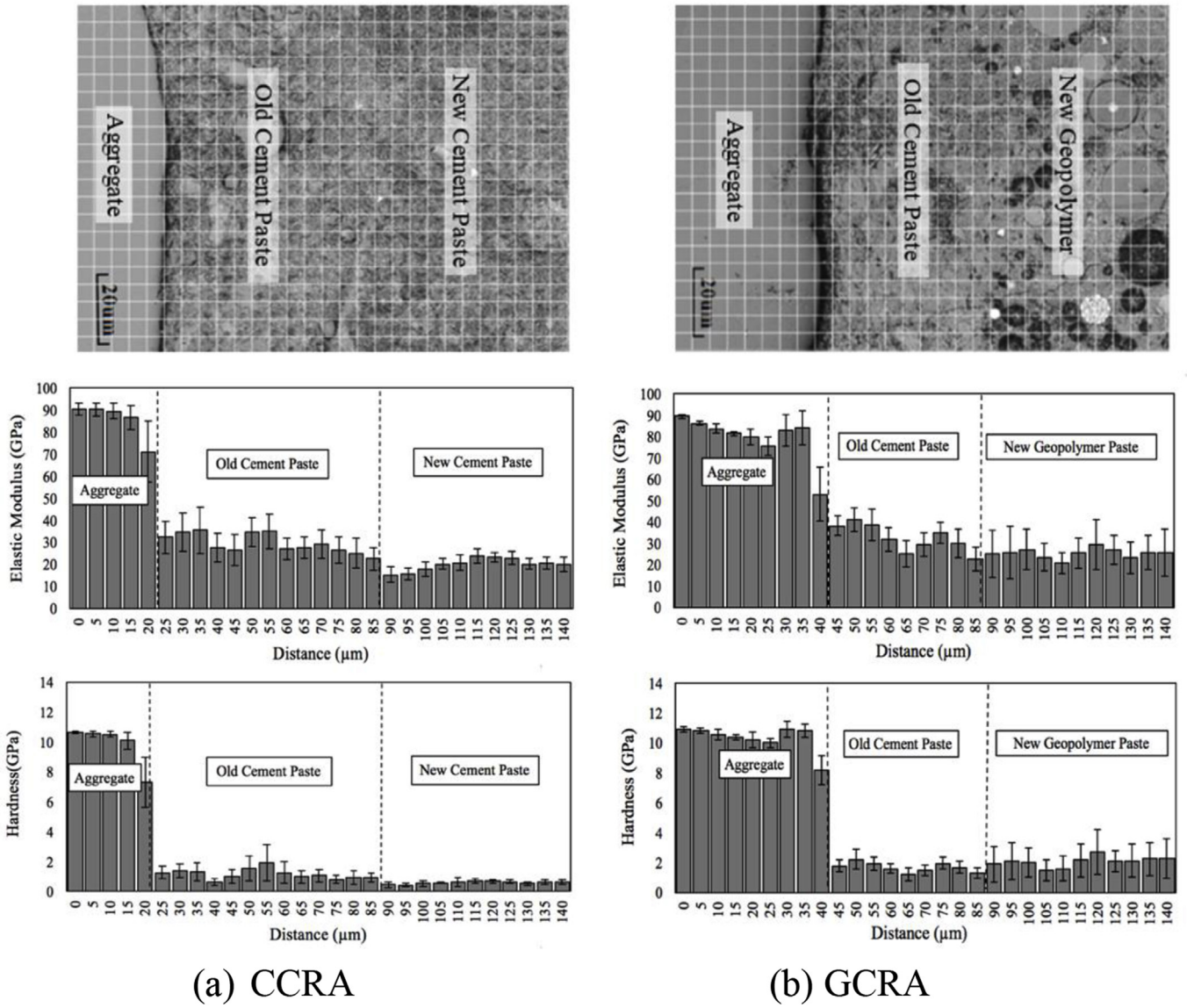

Fig. 7. Nanomechanical properties across aggregate-old paste-new paste.

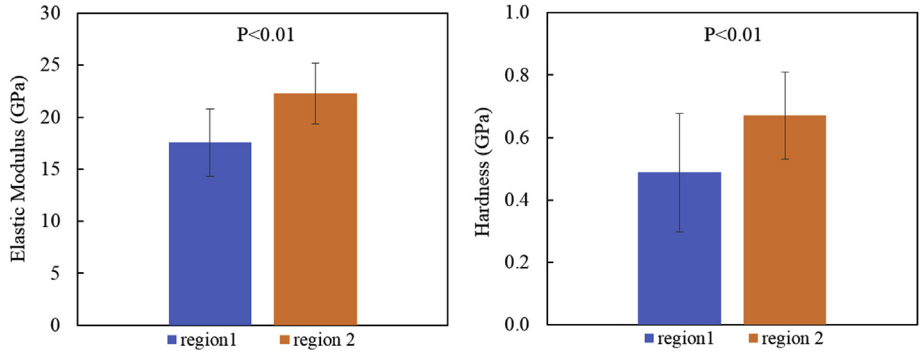

Fig. 8. Comparison of nanomechanical properties: region 1 (90 μm–110 μm) vs. region 2 (110 μm–140 μm) in new cement paste.

nanomechanical properties of the old interphase region in CCRA was similar to the properties of the adjacent paste when aggregate and paste were bonded well. However, the new interphase within a region approximately 20 μm from old cement paste in CCRA shows reduced mechanical properties, which correlates with the lower C-S-H content in this region.

When comparing the distribution profiles of Na in CCRA and GCRA, it is obvious that the old cement paste in GCRA contains much more Na than the old cement paste in CCRA. This result is interesting because cement paste usually contains a very low amount of Na. The nontrivial existence of Na detected from the old cement paste in GCRA implies that certain amounts of Na from the new geopolymer paste diffuse into

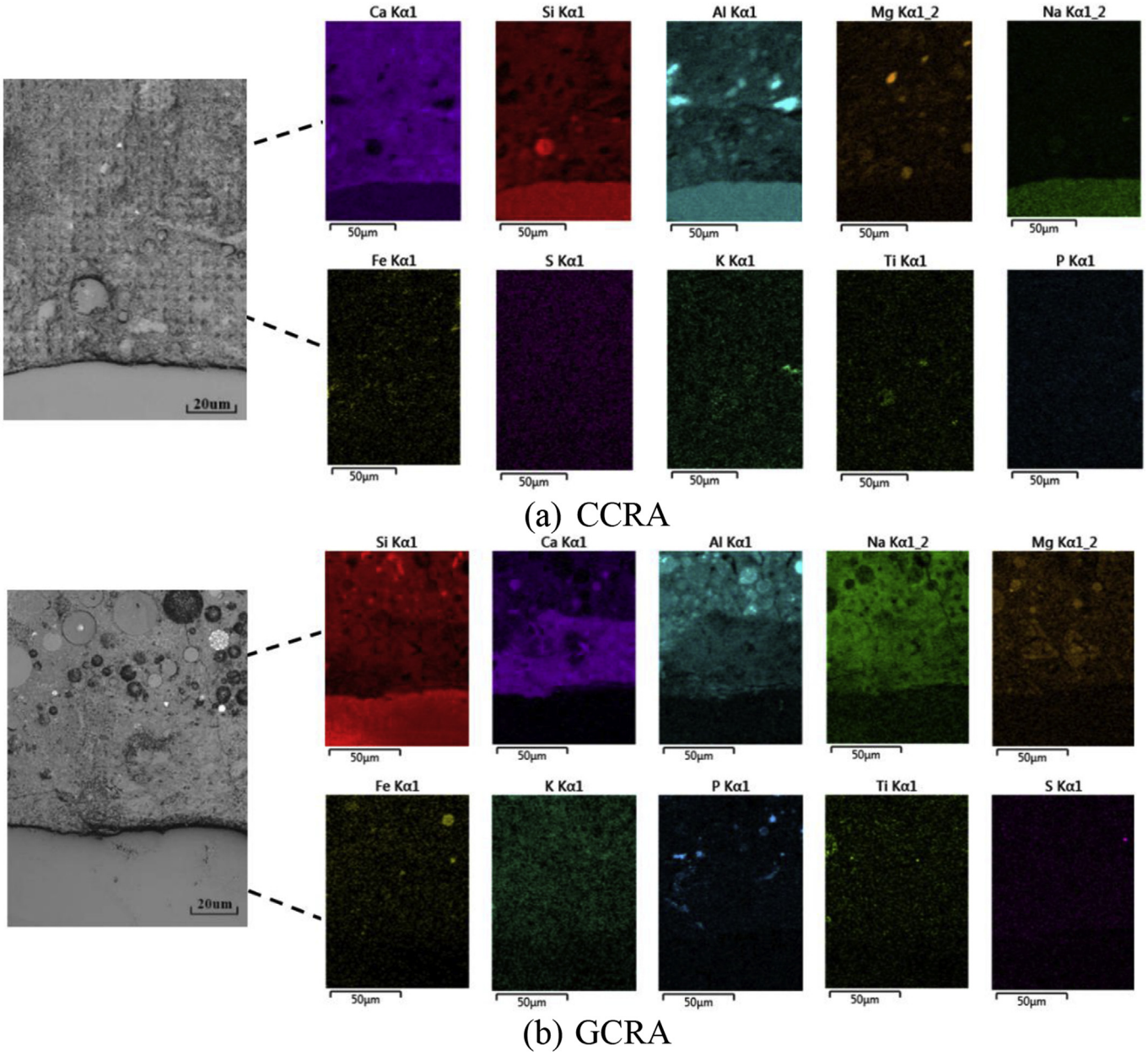

Fig. 9. EDS elemental maps.

the old cement paste. Further studies are needed to provide greater clarity to these results. In addition, the distribution profiles of three elements (Al, Si, and Na) along the distance from 95 to 105 μm show an abrupt increase in Na as well as the concentration of Al and Si. This behavior implies the existence of an interphase zone with an ample amount of N-A-S-H gel, which yields a strong bond between the old cement paste and new geopolymer paste. The increasing distribution of Si (the main element of fly ash) and decreasing trend of Na (the main element of N-A-S-H gel) throughout the new geopolymer paste (distance from 95 to 140 μm) indicate that more fly ash particles that were not fully reacted with the alkaline activator are placed further away from the surface of the old cement paste.

In order to investigate any possible effects of the geopolymer paste on the properties of the interphase in recycled aggregates, additional EDS analyses were conducted in two cases for comparisons: the interphase of old aggregate particles within an recycled aggregate without any interaction with new paste (Fig. 11) and the interphase of old aggregate particles within an recycled aggregate that shows interaction with the geopolymer paste (Fig. 12). Fig. 11 shows the LSM image with the region of interest (a box), its associated EDS chemical map showing all elements, and a scanning electron microscopy image identifying several specific zones to quantify the EDS results. At each zone, atomic Ca/Si ratios were obtained, and the results are presented in Table 2. The EDS analysis showed that there was a considerable difference in the Ca/Si ratios of the interphase (zones 1, 2, and 3) and the adjacent paste (zones 4, 5, and 6). It can clearly be seen that the Ca/Si ratio in the interphase is greater than that in the adjacent paste. The larger numbers of Ca/Si in the interphase are due to the presence of more Ca and less Si compared to the adjacent paste, which implies that the interphase region contains a higher content of CH crystals than in the adjacent paste.

The EDS maps shown in Fig. 12 are obtained from the regions in GCRA, in which the presence of the “unknown phase” (noted in Fig. 6) was detected. For comparison, four zones were chosen: zones 1 and 3 are considered the unknown phase in the vicinity of old aggregates and zones 2 and 4 are in the adjacent paste. Table 2 shows the EDS results. The elemental composition of all four zones was found to be dominated

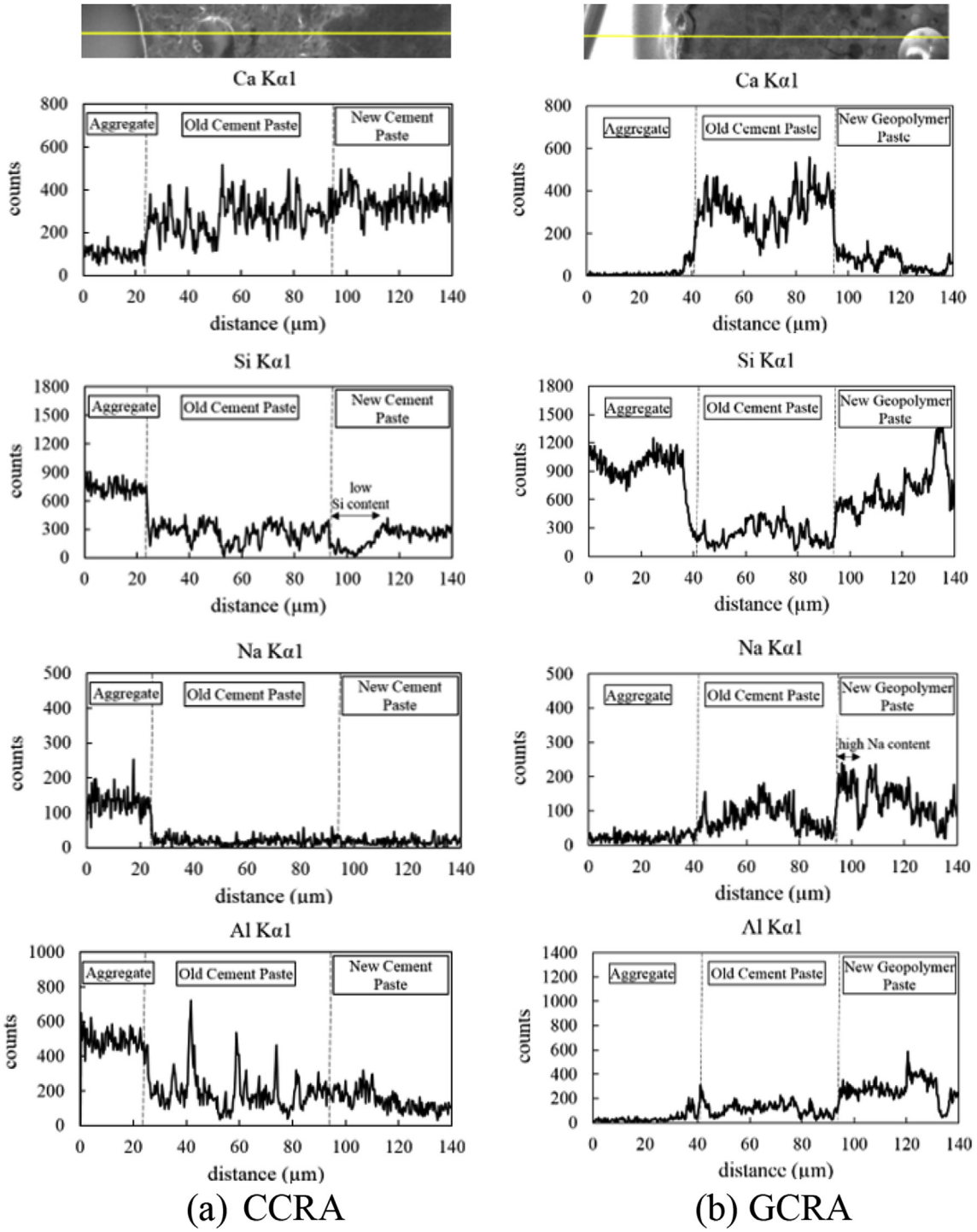

Fig. 10. EDS line scanning results across old and new interphase.

by Si, Ca, and Al. Comparing the two zones marked as the unknown phase, the concentration of each element was found to be quite similar. Consequently, the Ca/Si ratios of zones 1 and 3 are very similar. Comparing the two zones of adjacent paste (zones 2 and 4), the concentration of Si was quite similar. The resulting Ca/Si ratios of zones 2 and 4 were approximately 1.6 times greater than the ratios found from zones 1 and 3. According to other studies [47–49], the higher ratio of Ca/Si is caused by the intermixture of C-S-H with portlandite with CH possibly filling the interlayer space of C-S-H. The higher ratio of Ca/Si in zones 2 and 4 implies that the amount of CH crystals in the old cement paste is higher than that in the unknown phase. In addition, a lower Ca/Si ratio in the unknown phase could be due to the existence of more C-S-H in this region, which leads to the formation of more binding agent around the aggregate. The presence of highly cleavable and soluble CH crystals in the ITZ of recycled aggregates can lead to the formation of secondary C-S-H in the vicinity of the aggregate due to the pozzolanic reaction that occurs between CH crystals and the silica-rich fly ash. Other studies [50,51] found a similar observation from mixtures made with a combination of CH and metakoline-based geopolymer. It was found that when metakoline and CH were alkali-activated by NaOH, C-S-H gel was found to be the secondary product and the co-existence of the C-S-H and geopolymeric gel was not observed unless a

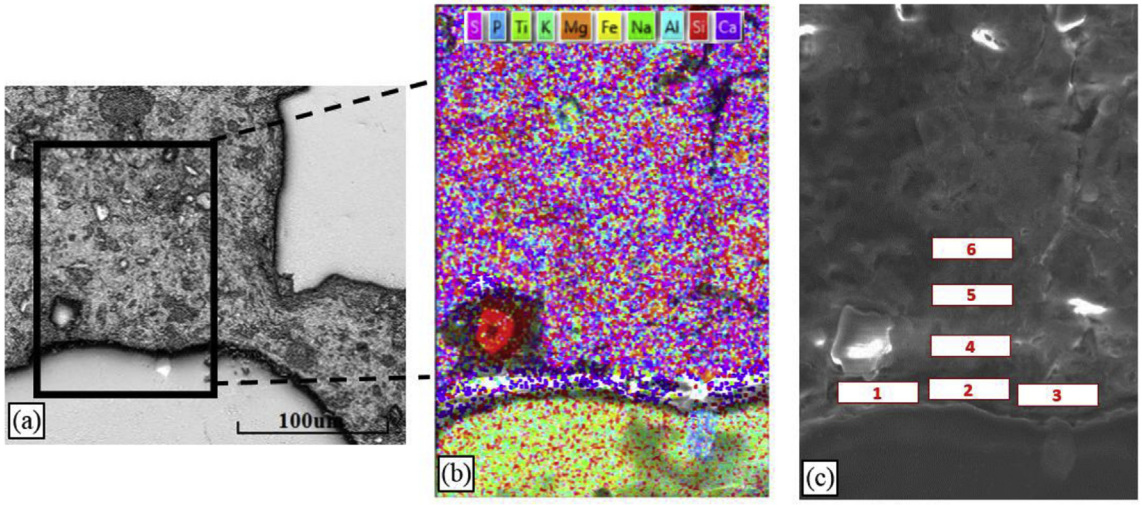

Fig. 11. EDS analysis of recycled aggregate: (a) region of interest; (b) EDS map; (c) zones for analysis.

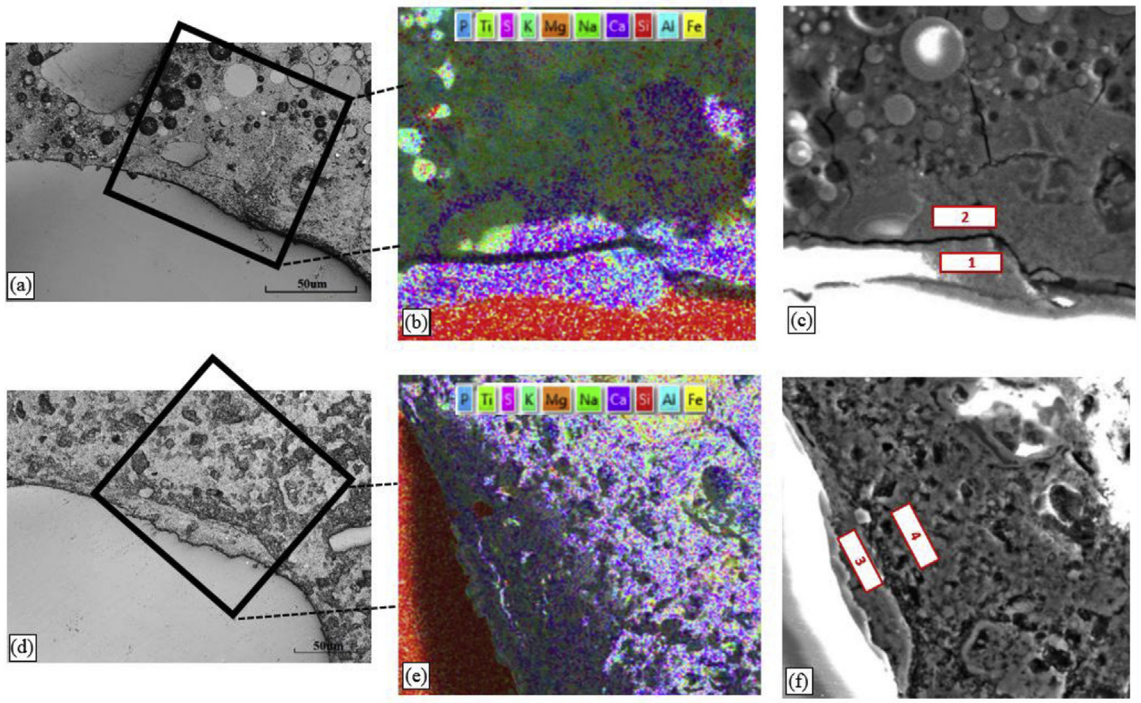

Fig. 12. EDS analysis of GCRA: (a), (d) typical microstructure with unknown phase in GCRA; (b), (e) EDS layered map; (c), (f) zones for analysis.

Table 2
EDS analysis results of the region of interest (interphase of old aggregate particles within a recycled aggregate without any interaction with new paste).

Region	Figure	Element Content (%)					
		Ca	Si	Al	Na	Other elements	Ca/Si
1	11	60.8	22.0	8.5	0	8.7	2.76
2	11	61.7	22.6	13.3	0	2.4	2.73
3	11	64.5	16.2	8.8	0	10.5	3.98
4	11	35.4	37.3	17.5	0	9.8	0.95
5	11	35.8	42.3	14.7	0	7.2	0.85
6	11	37.2	39.9	16.7	0	6.2	0.93

Table 3
EDS analysis results of the region of interest (interphase of old aggregate particles within a recycled aggregate interacted with geopolymer paste).

Region	Figure	Element Content (%)					
		Ca	Si	Al	Na	Other Elements	Ca/Si
1	12(c)	56.2	28.9	8.8	2.5	3.6	1.9
2	12(c)	56.4	19.1	12.2	9.1	3.2	3.0
3	12(f)	54.0	28.5	8.8	5.1	3.6	1.9
4	12(f)	62.2	19.7	7.5	5.1	5.5	3.1

reactive calcium source was initially present. In contrast, as can be seen in Table 3, all zones in the old cement paste contain Na, while the recycled aggregates did not show any Na content (see Table 2). This observation confirms that the geopolymer paste influenced and changed the old paste characteristics, which resulted in an increased Na content and new product that filled the separated interphase between the old aggregates and old cement paste.

6. Concluding remarks

Recycled aggregates were mixed with two different cementitious materials, OPC and fly ash-based geopolymer, and the interphase characteristics in those cementitious composites were investigated by integrating multiscale tests and analyses. The microstructural, nanomechanical, and chemical properties were identified by laser scanning microscopy, nanoindentation, and SEM–EDS, respectively. The following conclusions can be obtained from this study results:

- In cement concrete mixtures with recycled aggregates, a pre-existing incomplete interphase was observed within the recycled aggregates, although the new paste was relatively well-bonded to the old paste by having an ITZ approximately 20-μm-thick.
- In geopolymer concrete mixtures with recycled aggregates, both old and new interphases appeared dense. More interestingly, the pre-existing incomplete interphase of old aggregate particles within the recycled aggregates was filled, which was not the case observed in the cement concrete with recycled aggregates.
- Further analysis through EDS indicated that geopolymeric materials can reach the pre-existing incomplete interphase and create geopolymerization-hydration products that combine the sodium aluminosilicate hydrate (N-A-S-H) gel and calcium-silicate-hydrate (C-S-H).
- Based on the test-analysis results, it can be inferred that the fly ash-based geopolymer is well suited for use with recycled aggregates with enhanced mechanical properties, which can lead to engineering of greener cementitious composites. However, this research outcome should be verified with more test results and investigations. Such further efforts are under progress by the authors, and follow-up results will be presented when available.

Compliance with ethical standards

Ethical responsibilities of authors

This manuscript represents original work that is not being considered for publication, in whole, in another journal, book, conference proceedings, or government publication. All previously published work cited in the manuscript has been fully acknowledged. This manuscript is one of a kind, or part of a study or thesis from which other manuscripts may be generated. All of the authors have contributed substantially to the manuscript and approved the final submission.

Conflict of interest

The authors declare that they have no conflict of interest.

Acknowledgements

We acknowledge the financial support from the National Science Foundation (Grant No. CMMI-1635055) for this study. We also like to acknowledge testing facilities: the Nano-Engineering Research Core Facility (NERCF) and the Nebraska Center of Materials and Nanoscience (NCMN) at the University of Nebraska-Lincoln where the laboratory tests for this study were performed.

Appendix A. Supplementary data

Supplementary data to this article can be found online at https://doi.org/10.1016/j.compositesb.2018.09.041.

References

[1] Meyer C. The greening of the concrete industry. Cement Concr Compos 2009;31(8):601–5.
[2] Casuccio M, Torrijos M, Giaccio G, Zerbino R. Failure mechanism of recycled aggregate concrete. Construct Build Mater 2008;22(7):1500–6.
[3] Poon C, Shui Z, Lam L, Fok H, Kou S. Influence of moisture states of natural and recycled aggregates on the slump and compressive strength of concrete. Cement Concr Res 2004;34(1):31–6.
[4] Shayan A, Xu A. Performance and properties of structural concrete made with recycled concrete aggregate. ACI Mater. J. Am. Concr. Inst. 2003;100(5):371–80.
[5] Xiao J, Li W, Poon C. Recent studies on mechanical properties of recycled aggregate concrete in China—a review. Sci China Technol Sci 2012;55(6):1463–80.
[6] Tabsh SW, Abdelfatah AS. Influence of recycled concrete aggregates on strength properties of concrete. Construct Build Mater 2009;23(2):1163–7.
[7] Olorunsogo F, Padayachee N. Performance of recycled aggregate concrete monitored by durability indexes. Cement Concr Res 2002;32(2):179–85.
[8] Katz A. Properties of concrete made with recycled aggregate from partially hydrated old concrete. Cement Concr Res 2003;33(5):703–11.
[9] Rao A, Jha KN, Misra S. Use of aggregates from recycled construction and demolition waste in concrete. Resour Conserv Recycl 2007;50(1):71–81.
[10] Ajdukiewicz A, Kliszczewicz A. Influence of recycled aggregates on mechanical properties of HS/HPC. Cement Concr Compos 2002;24(2):269–79.
[11] Malhotra V. Role of supplementary cementing materials in reducing greenhouse gas emissions. Infrastructure regeneration and rehabilitation improving the quality of life through better construction. International conference. 1999. p. 27–42.
[12] Hardjito D, Wallah SE, Sumajouw DM, Rangan BV. On the development of fly ash-based geopolymer concrete. Mater. Journal 2004;101(6):467–72.
[13] Hardjito D, Wallah SE, Sumajouw DM, Rangan BV. Fly ash-based geopolymer concrete. Aust J Struct Eng 2005;6(1):77–86.
[14] Duxson P, Provis JL, Lukey GC, Van Deventer JS. The role of inorganic polymer technology in the development of 'green concrete'. Cement Concr Res 2007;37(12):1590–7.
[15] van Deventer JS, Provis JL, Duxson P, Brice DG. Chemical research and climate change as drivers in the commercial adoption of alkali activated materials. Waste Biomass Valorization 2010;1(1):145–55.
[16] Gourley J, Johnson G. Developments in geopolymer precast concrete. World congress geopolymer. 2005.
[17] Majidi B. Geopolymer technology, from fundamentals to advanced applications: a review. Mater Technol 2009;24(2):79–87.
[18] Rangan BV, Hardjito D, Wallah SE, Sumajouw DM. Properties and applications of fly ash-based concrete. Mater Forum 2006;30:170–5.
[19] Ryu GS, Lee YB, Koh KT, Chung YS. The mechanical properties of fly ash-based geopolymer concrete with alkaline activators. Construct Build Mater 2013;47:409–18.
[20] Temuujin J, van Riessen A, MacKenzie K. Preparation and characterisation of fly ash based geopolymer mortars. Construct Build Mater 2010;24(10):1906–10.
[21] Khedmati M, Kim Y-R, Turner JA, Alanazi H, Nguyen C. An integrated microstructural-nanomechanical-chemical approach to examine material-specific characteristics of cementitious interphase regions. Mater Char 2018;138:154–64.
[22] Rami KZ, Kim Y-R, Khedmati M, Nsengiyumva G, Alanazi H. Two-way linked multiscale method integrated with nanomechanical tests and cohesive zone fracture to model highly heterogeneous binding materials. J Eng Mech 2018;144(10):04018095.
[23] Akçaoğlu T, Tokyay M, Çelik T. Assessing the ITZ microcracking via scanning electron microscope and its effect on the failure behavior of concrete. Cement Concr Res 2005;35(2):358–63.
[24] Diamond S, Huang J. The ITZ in concrete–a different view based on image analysis and SEM observations. Cement Concr Compos 2001;23(2):179–88.
[25] Gao Y, De Schutter G, Ye G, Huang H, Tan Z, Wu K. Porosity characterization of ITZ in cementitious composites: concentric expansion and overflow criterion. Construct Build Mater 2013;38:1051–7.
[26] Scrivener KL, Crumbie AK, Laugesen P. The interfacial transition zone (ITZ) between cement paste and aggregate in concrete. Interface Sci 2004;12(4):411–21.
[27] Stutzman PE. Scanning electron microscopy in concrete petrography vol. 2. National Institute of Standards and Technology; 2001.
[28] Tam VW, Gao X, Tam CM. Microstructural analysis of recycled aggregate concrete produced from two-stage mixing approach. Cement Concr Res 2005;35(6):1195–203.
[29] Xiao J, Li W, Corr DJ, Shah SP. Effects of interfacial transition zones on the stress–strain behavior of modeled recycled aggregate concrete. Cement Concr Res 2013;52:82–99.
[30] Xiao J, Li W, Sun Z, Lange DA, Shah SP. Properties of interfacial transition zones in recycled aggregate concrete tested by nanoindentation. Cement Concr Compos 2013;37:276–92.
[31] Etxeberria M, Vázquez E, Mari A. Microstructure analysis of hardened recycled aggregate concrete. Mag Concr Res 2006;58(10):683–90.
[32] Nagataki S, Gokce A, Saeki T, Hisada M. Assessment of recycling process induced damage sensitivity of recycled concrete aggregates. Cement Concr Res 2004;34(6):965–71.
[33] Khan A. Recycled concrete—a source for new aggregate. Cem Concr Aggregates 1984;6(1):17–27.
[34] Lee G, Choi H. Study on interfacial transition zone properties of recycled aggregate by micro-hardness test. Construct Build Mater 2013;40:455–60.
[35] Liu Z, Cai C, Peng H, Fan F. Experimental study of the geopolymeric recycled aggregate concrete. J Mater Civ Eng 2016;28(9):04016077.
[36] Shi XS, Collins FG, Zhao XL, Wang QY. Mechanical properties and microstructure analysis of fly ash geopolymeric recycled concrete. J Hazard Mat 2012;237:20–9.
[37] Shi XS, Wang QY, Zhao XL, Collins FG. Discussion on properties and microstructure of geopolymer concrete containing fly ash and recycled aggregate. Adv Mat Res

2012;450. Trans Tech Publications.
[38] Miller M, Bobko C, Vandamme M, Ulm F-J. Surface roughness criteria for cement paste nanoindentation. Cement Concr Res 2008;38(4):467–76.
[39] Kjellsen K, Monsøy A, Isachsen K, Detwiler R. Preparation of flat-polished specimens for SEM-backscattered electron imaging and X-ray microanalysis—importance of epoxy impregnation. Cement Concr Res 2003;33(4):611–6.
[40] Haghshenas HF, Kim Y-R, Morton MD, Smith T, Khedmati M, Haghshenas DF. Effect of softening additives on the moisture susceptibility of recycled bituminous materials using chemical-mechanical-imaging methods. J Mater Civ Eng 2018;30(9):04018207.
[41] Sandak J, Tanaka C. Evaluation of surface smoothness by laser displacement sensor 1: effect of wood species. J Wood Sci 2003;49(4):305–11.
[42] Zou Y, Kaestner M, Reithmeier E. A method for multi-resolution characterization on porous surfaces by using a laser confocal scanning microscope. Optic Laser Eng 2015;74:40–6.
[43] Němeček J. Creep effects in nanoindentation of hydrated phases of cement pastes. Mater Char 2009;60(9):1028–34.
[44] Oliver WC, Pharr GM. An improved technique for determining hardness and elastic modulus using load and displacement sensing indentation experiments. J Mater Res 1992;7(6):1564–83.
[45] Pichler C, Lackner R. Upscaling of viscoelastic properties of highly-filled composites: investigation of matrix–inclusion-type morphologies with power-law viscoelastic material response. Compos Sci Technol 2009;69(14):2410–20.
[46] Monteiro J, Mehta PK. Ettringite formation on the aggregate—cement paste interface. Cement Concr Res 1985;15(2):378–80.
[47] Pardal X, Pochard I, Nonat A. Experimental study of Si–Al substitution in calcium-silicate-hydrate (CSH) prepared under equilibrium conditions. Cement Concr Res 2009;39(8):637–43.
[48] Grangeon S, Fernandez-Martinez A, Baronnet A, Marty N, Poulain A, Elkaïm E, Roosz C, Gaboreau S, Henocq P, Claret F. Quantitative X-ray pair distribution function analysis of nanocrystalline calcium silicate hydrates: a contribution to the understanding of cement chemistry. J Appl Crystallogr 2017;50(1):14–21.
[49] Garbev K, Bornefeld M, Beuchle G, Stemmermann P. Cell dimensions and composition of nanocrystalline calcium silicate hydrate solid solutions. Part 2: X-ray and thermogravimetry study. J Am Ceram Soc 2008;91(9):3015–23.
[50] Alonso S, Palomo A. Alkaline activation of metakaolin and calcium hydroxide mixtures: influence of temperature, activator concentration and solids ratio. Mater Lett 2001;47(1–2):55–62.
[51] Yip CK, Lukey G, Van Deventer J. The coexistence of geopolymeric gel and calcium silicate hydrate at the early stage of alkaline activation. Cement Concr Res 2005;35(9):1688–97.